Carboxylic Acid-Functionalized Conjugated Polymer Promoting Diminished Electronic Drift and Amplified Proton Sensitivity of Remote Gates Compared to Nonpolar Surfaces in Aqueous Media

Hyun-June Jang, Justine Wagner, Yunjia Song, Taein Lee, and Howard E. Katz

Department of Materials Science and Engineering, Johns Hopkins University, 3400 N. Charles St, Baltimore, USA

Keywords:

Conjugated polymers, P3HT, poly(3-carboxypropylthiophene), remote gate FET, drift, pH sensitivity

Abstract

A systematic analysis was used to understand electrical drift occurring in field-effect transistor (FET) dissolved-analyte sensors by investigating its dependence on electrode surface-solution combinations in a remote-gate (RG) FET configuration. Water at pH 7 and neat acetonitrile, having different dipoles and polarizabilities, were applied to the RG surface of indium tin oxide (ITO), SiO_2, hexamethyldisilazane-modified SiO_2, polystyrene, poly(styrene-co-acrylic acid), poly(3-hexylthiophene-2,5-diyl) (P3HT), and poly [3-(3-carboxypropyl)thiophene-2,5-diyl] (PT-COOH). We discovered that in some cases a slow reorientation of dipoles at the interface induced by gate electric fields caused severe drift and hysteresis because of induced interface potential changes. Conductive and charged P3HT and PT-COOH increased electrochemical stability by promoting fast surface equilibrations. We also demonstrated pH sensitivity of P3HT (17 mV/pH) as an indication of proton doping. PT-COOH showed further enhanced pH sensitivity (30 mV/pH). This combination of electrochemical stability and pH response in PT-COOH are proposed as advantageous for polymer-based biosensors.

Field-effect transistor (FET) biosensors inevitably contain a solution interface contact on the sensing material where receptors for dissolved biomarkers are placed. A solution interface under the influence of an electric field (E_F) is a source of electrochemical instability (potential drift) that challenges real-time diagnostics by affecting device sensitivity, specificity, and limit-of-detection. Drift (ΔV_{dri}) in n-FETs exhibited as a slow, monotonic, and temporal increase in threshold voltage (V_{th}) from the initial V_{th} (V_{th0}) to saturation point (V_{sat}) has been shown as a common behavior over a diverse range of sensing materials[1-3]. This can arise from slow response of buried surface sites[1], the injection of electrons[2], and accumulation and migration of ions[3]. Commonalities in drift observations could suggest related roles of solutions in drift[4]. In recent molecular dynamic simulations, dipoles in the solution are found to be oriented on the surface by the applied E_F (saturation effect)[5] leading to inhomogeneous dielectric permittivity (ε_r) of the solution, which occurs even on hydrophobic surfaces[6-8]. This orientational ordering at the interface gives rise to a steep reduction of ε_r[6, 7, 9-11] and double layer capacitance (C_{DL})[8, 12], as well as charge screening[12]. Organic materials show larger drift components compared to inorganic surfaces[13]. Nonetheless, transparency, flexibility, and integrability with textiles and skin are valuable attributes of organic materials for wearable electronics [14]. Recently, conjugated polymers have received considerable attention as active sensing layers for organic electrochemical transistors (OECTs)[15] due to enhanced stability, long lifetime, and fast response for voltage cycles in ionic liquids[16]. Progress requires better understanding of the mechanistic factors behind drift. It is challenging to discriminate the kinetics of dipole moment orientations on the surface of a conjugated polymer with an OECT structure because the drain current of an OECT is determined by multiple species such as hole carriers, mobile ions in solutions, ions that diffuse into conjugated polymers, interface traps between material interfaces, and products of redox reactions.

Meanwhile, the remote-gate FET (RGFET), in which a sensitive surface is integrated with a commercial Si-FET (Figure 1), only translates the surface potential (ψ_s) of RG material to the gate of

the Si-FET[17] due to the high input impedance of the Si-FET (Figure S1). Thus, the RGFET is advantageous for the investigations of solution interfaces as a function of dipole moments and specific surface responses to the dipole moments. To be specific, the electrical potential of a solution interface can be analyzed by measuring changes in V_{th} and transconductance (G_m) of RGFETs relative to those of the Si-FET: V_{th} (1.5 V) and G_m (66 μS) of the Si-FET remain consistent over all our experiments (Figure S1). These are defined as V_{FET} and G_{FET}, respectively.

In this paper, we connect ΔV_{dri}, drift in G_m (ΔG_{dri}), and hysteresis in V_{th} (ΔV_{hys}) and in G_m (ΔG_{hys}) to slow dipole rearrangement at the interface by discovering a dependency between electric charges of RG surfaces and dipole moments of the solution on the solution interface. ΔV_{hys} and ΔG_{hys} herein are a difference in V_{th} and G_m between FSM and reverse sweep mode (RSM). Different dipole moments from a pH7 aqueous buffer solution and an organic solvent acetonitrile (ACN) were initially applied on various surfaces (Figure 1) including indium tin oxide (ITO), SiO_2, hexamethyldisilazane (HMDS), polystyrene (PS), and poly(styrene-co-acrylic acid) (PSAA, 60% PS).

The ITO surface represents a highly stable inorganic surface in an aqueous solution. In contrast, a hydrophilic SiO_2 surface induces severe drift especially stemming from slow hydration of buried hydroxyl sites underneath SiO_2 surfaces[18, 19]. HDMS and PS layers deposited on SiO_2 exhibit properties of hydrophobic surfaces including severe electrochemical instability. A PSAA layer is amphiphilic but its backbone is non-conductive. PSAA reveals severe instability in a pH7 solution but presents insignificant ΔV_{dri} and ΔV_{hys} in a non-polar ACN solution since the chargeable groups inducing orientations of ACN dipoles create less dipolar polarization at the interface. In contrast, poly(3-hexylthiophene-2,5-diyl) (P3HT) that has many mobile positive charges from poly-thiophene backbones shows enhanced stability in the aqueous solution although its surface is hydrophobic. Moreover, poly [3-(3-carboxypropyl)thiophene-2,5-diyl] (PT-COOH) shows even higher stability than P3HT in an aqueous solution.

For the RGFET analysis, V_{th0} and V_{sat} are an indication of the initial interfacial potential ψ_s and the final ψ_s affected by dipole orientations at quasi-equilibrium, respectively. If V_{th0} of the RGFETs is higher than V_{FET}, we state that the RG initially imposes negative electrical potentials on the gate of the Si-FET and vice versa, because positive voltage turns on the n-type Si-FET.

The ITO surface shows stable V_{th} and G_m in both ACN (1.8 V, 65.8 μS) and pH7 solution (1.54 V, 64.8 μS) with no observable ΔV_{dri}, ΔV_{hys}, ΔG_{dri}, or ΔG_{hys} (Figure S2). Initial G_m (G_{m0}) only decreases by 0.3 % in ACN and 1.8 % in pH7 compared to G_{FET}. High pH sensitivity (52 mV/pH, close to Nernstian with 99.7% linearity) was reversible with no ΔG_{dri} or ΔG_{hys} (Figure S3).

The typical drift characteristics are presented from SiO_2, HMDS, PS, and PSAA surfaces in pH7 water in orange-colored data over Figure 2a-2d. Three of the systems showed slow evolution of V_{th0} to V_{sat}. Each transfer curve is shown in Figure S4. Divergent V_{th0} of each RG converges to a similar range in V_{sat} (SiO_2: 1.86 V, HMDS: 1.83 V PS: 1.84 V, PSAA: 1.8 V), indicating an achievement of similar ψ_s from dipole orientations induced by the same voltage biasing conditions. When gate E_F is disconnected, each V_{th0} recovers quickly while reversible drift curves are obtained. This could be explained as dipoles being slowly and temporarily anchored at the interface only as a result of applied E_F schmatically shown in Figure 2e.

ΔV_{dri} and ΔG_{dri} is further referenced to V_{th0} and G_{FET}, respectively. Large ΔV_{dri} (8%) is observed in SiO_2 surface due to slowly hydrated surfaces (Figure 2a). However, G_{m0} of hydrophilic SiO_2 (64.2 μS) only decreases by 2.7% relative to G_{FET} with a small ΔG_{dri} of 3.3%. Similar ΔV_{dri} are repeated over pH3 to 11 solutions resulting in the limited SiO_2 pH sensitivity of 2 mV/pH (Figure S5a). G_m also varies depending on pH of solutions (Figure S5b). This shows the drift from hydration is associated with a low pH sensitivity of SiO_2.

Both HMDS (Figure 2b) and PS (Figure 2c) present a larger ΔV_{dri} of 17% due to a competing relation between hydrophobic surface-solution interactions. Unstable orientational ordering is enforced

by the applied gate E_F schmatically shown in Figure 2f. Accordingly, G_{m0} of HMDS (61.3 μS) and PS (56.3 μS) is largely reduced by 7.1 % and 14.7% with a large ΔG_{dri} of 8.3 % and 16%, respectively. PSAA incorporating ionizable COOH reduces ΔV_{dri} (11%), compared to that of PS (17%), shown in the second measurement cycle (Figure 2d). It is noted that a large ΔV_{dri} of PSAA at the first measurement cycle possibly included the initial equilibration of PSAA with the pH of the solution (Figure S6). Moreover, the charged components in PSAA schematically shown in Figure 2g increase G_{m0} (61.1 μS) by 7% compared to PS (56.3 μS). Still, the hydrated structure in PSAA limits pH sensitivity to 5.4 mV/pH with a large ΔG_{dri} and ΔG_{hys} varying with the pH of solutions (Figure S6).

ΔV_{hys} observed by RSM (gray-colored data over Figure 2a-2d) that immediately started after the end of FSM is related to slow response of additional dipoles to the high, positive gate voltage and to dipoles already oriented by the FSM at the interface schmatically shown in Figure 2h. ΔV_{hys} and ΔG_{hys} are referenced to V_{th} and G_m at FSM, respectively. The confinement of additional dipoles at the interface by RSM increases G_m at RSM of 1.2%, 1.9%, 7.4%, 1.4% for SiO_2, HMDS, PS, and PSAA, respectively, indicating high voltage dependency of G_m from these evolving interfaces. The most hydrophobic surface was associated with higher ΔV_{hys} (HMDS: 6.8%, PS: 24%, PSAA: 11%, SiO_2: 2.2%).

The same measurements were applied for each surface RG above but switching to ACN with lower dipole moment as shown in Figure 3a, 3b and Figure S7. ACN always offers higher G_{m0} than those in pH7 water inferring less influence of ACN dipoles at the interface than pH7 solution (Figure S8). A large ΔV_{dri} and ΔV_{hys} of SiO_2 and PSAA shown in pH7 are highly alleviated in ACN (Figure S7) while G_{m0} only decreases by 0.6% (w/ ΔG_{dri} of 3.1 %) for SiO_2 and 3.4% (w/ ΔG_{dri} of 3.7%) for PSAA, respectively. ΔV_{dri} and ΔV_{hys} of PS (25%, 3%) and HMDS (19%, 10%), however, are still pronounced. These systems show unique reversible drift curves: trivial ΔV_{hys} during drift and increased ΔV_{hys} after drift (Figure 3a, 3b). This could be interpreted as repeating gate voltage cycles develop orientational ordering of ACN dipoles causing drift which in turn triggered hysteresis as described in Figure 2h. After

drift, high G_{m0} of PS (64.6 μS) and HMDS (62.7 μS) are further reduced by 3.6% and 6%, respectively. In the summarized V_{th0} and V_{sat} for each RG (Figure 3c), non-polar surfaces of PS and HMDS had a similar V_{th0} (PS:1.5 V, HMDS: 1.52 V). Also, their V_{sat} levels converged to a specific range (PS: 1.89 V, HMDS: 1.82 V) as was the case in pH7 water. Charged components seem to suppress ΔV_{hys} and ΔV_{dri} (Figure 3d). ΔG_{dri} and ΔG_{hys} (Figure 3e) seem to arise from unstable dipole orientations at non-polar surfaces.

Our observations so far, particularly those on ITO compared to the other RG materials and the reduced hysteresis of PSAA compared to PS, give rise to a clear criterion in designing a polymer sensing layer using charged and conductive components for greater electrochemical stability. The positively charged P3HT surface shows highly reduced ΔV_{dri} of 1%, ΔV_{hys} of 0.3 % (but initial slight drift in V_{th}), and high stable G_{m0} of 64.3 μS with no ΔG_{dri} and ΔG_{hys} (Figure 4a, Figure S9a) although the P3HT layer is hydrophobic. PT-COOH proposed for a biosensing layer shows enhanced stability with ΔV_{dri} of 0.01% and no ΔV_{hys} (Figure 4b, Figure S9b), which is almost comparable to those of ITO (Figure S1d).

Without any leakage current through the P3HT RG (Figure S10), reversible pH sensitivity of 17 mV/pH ranging from pH3 to 10 was obtained (Figure 4c, Figure S11a). This possibly comes from ionic proton doping effects in the amorphous domains of poly-thiophene[15, 20-22]. Much higher pH sensitivity of 30 mV/pH (Figure 4d, Figure S11b) with no ΔG_{dri} and ΔG_{hys} is achieved from of PT-COOH, becoming closer to the pH sensitivity of ITO and about half the Nernstian sensitivity. Enhanced pH response is observed for acidic solutions compared to that of P3HT (Figure 4e). For strongly basic solutions from pH9 to 11, fluctuations in V_{th} are observed for both materials (Figure 4c, 4d). Possibly, OH^- ions could be reactive with the polythiophene while some slow equilibration followed an initial penetration of OH^- ions.

Our findings are summarized by plotting the V_{th0} (Figure 3f) and V_{sat} (Figure 3g) of each RG surface in pH7 water. High V_{th0} of SiO_2 (1.7 V) and low V_{th0} of P3HT (1.43 V) reflect the negatively

and positively charged surface in pH7 water, respectively. Despite different thicknesses of films (HMDS: < 5 nm, PS: ca. 100 nm), V_{th0} of PS (1.55 V) and HMDS (1.56 V) is in a similar range as was also observed in ACN, indicating that the RGFET mostly translated the interface potentials[17]. Similar V_{sat} values for non-conductive surfaces indicated similar ψ_s after drift once initially unstable solvent dipole orientations were equilibrated (Figure 3g). Conductive surfaces show insignificant differences between V_{th0} and V_{sat}. Also, the trend of ΔV_{dri} and ΔV_{hys} in pH7 water (Figure 4h) corresponds to that of ΔG_{dri} and ΔG_{hys} (Figure S12) as was true in ACN. Finally, high pH sensitivity of PT-COOH (Figure 4i) is indicative of the surface accessibility and participation of a significant number density of COOH groups. Such sites could be electronically sensitive anchor points for bioreceptors.

In summary, we investigated how drift and hysteresis varied according to different surface polarities and solution dipole moments in an RGFET system. Fast, stable orientational ordering of dipoles on charged surfaces increased electrochemical stability. Therefore, charged conjugated polymers with physical stability in aqueous solution are recommended for use in biosensing layers. We demonstrated that P3HT and PT-COOH had superior electrochemical stability, almost comparable to that of ITO. Also, the pH sensitivity of P3HT (17 mV/pH) is demonstrated, presumably occurring by ionic doping. To the best of our knowledge, this is the first reported observation of the reversible proton sensitivity of P3HT only in terms of changes in the surface potential of P3HT as a sensing layer on the gate. The pH sensitivity of PT-COOH is further increased due to the incorporation of additional ionizable functionalities (30 mV/pH). Our results suggest a criterion in designing new polymers for biosensing interfaces requiring receptor attachment combining conjugation and charged components in the materials in order to rapidly equilibrate solution dipole moments with the applicatoin of E_F. This criterion is in fact met by PEDOT-PSS[23] and related polymers now used in organic electrochemical transistors, and is now suggested even for sensing layers that interact with analytes purely by polarization mechanisms.

Experimental Section

ITO/PET (Sigma Aldrich, 639303) was sliced (1× 2 cm) for the RG and was cleaned with isopropanol for 20 min under ultrasonication, rinsed with distilled water for 20 min. A standard RCA cleaning process was applied for the same sized SiO_2/Si substrates with 300 nm thickness of oxide. HMDS was deposited on the SiO_2 substrate via vacuum baking at 120 °C for 2 hours and then the samples were sonicated for 15 min in hexane and followed by IPA. A solution of 35 mg/ml of PS was prepared by dissolving the polymer in chloroform. PS was spin coated on the SiO_2 substrate at 1500 RPM for 1 min. PS/SiO_2 RG was baked at 120 °C for 2 hours for solvent outgassing. PSAA solution was prepared at concentration of 10 mg/ml in tetrahydrofuran and was spin coated on the SiO_2 substrate at 1500 RPM for 1 min. PSAA/SiO_2 RG was baked at 80 °C for 2 hours. A concentration of 10 mg/ml of P3HT and PT-COOH were prepared by dissolving each polymer in chlorobenzene and dimethylformamide, respectively. The prepared solutions were then sonicated for 1 hour and then heated at 60 °C overnight for making the polymer fully dissolved while the PT-COOH required the temperature to be raised to 115°C for 20 minutes. P3HT and PT-COOH were then spin coated on SiO_2/Si under 1600 RPM for 1 min and 1600 RPM for 5 min, respectively. P3HT/SiO_2 and PT-COOH/SiO_2 RG was baked at 80 °C for 2 hours. All concentrated solutions were filtered using a hydrophobic PTFE or hydrophilic PTFE syringe filter before spincoating. A commercial FET (CD4007UB) was used as a transducer to investigate fabricated RGs above. Aqueous solution at defined pH or ACN was placed on each RG surface. A Ag/AgCl reference electrode was placed in the solution in order to apply the gate bias for all measurements. All transfer curves were measured by using a Keithley semiconductor analyzer with a drain voltage set at 50 mV and the gate voltage left at double sweep mode. pH sensitivity of each RG surface was evaluated by using standard pH buffer solution. V_{th} is calculated as the gate voltage corresponding to drain current of 1 μA in each transfer curve.

Supporting Information

Supporting Information is available from the Wiley Online Library or from the author.

Acknowledgements

This work was primarily supported by the National Science Foundation, Division of Materials Research, Biomaterials Program, Grant number 1807292. The participation of Taein Lee was supported by the National Science Foundation DMREF program, grant number 1728947.

Conflict of Interest

The authors declare no conflict of interest.

References

[1] S. Jamasb, S. Collins, R. L. Smith, *Sens. Actu. B* **1998**, *49*, 146.

[2] Nicollia.Eh, C. N. Berglund, P. F. Schmidt, J. M. Andrews, *J. Appl. Phys*. **1971**, *42*, 5654.

[3] E. Cabruja, A. Merlos, C. Cane, M. Lozano, J. Bausells, J. Esteve, *Surf. Sci.* **1991**, *251*, 364.

[4] E. Bjornehohn, M. H. Hansen, A. Hodgson, L. M. Liu, D. T. Limmer, A. Michaelides, P. Pedevilla, J. Rossmeisl, H. Shen, G. Tocci, E. Tyrode, M. M. Walz, J. Werner, H. Bluhm, *Chem. Rev.* **2016**, *116*, 7698.

[5] F. Booth, J. *Chem. Phys.* **1951**, *19*, 391.

[6] T. Sato, T. Sasaki, J. Ohnuki, K. Umezawa, M. Takano, *Phys. Rev. Lett.* **2004**, *93*, 206002.

[7] F. Despa, A. Fernandez, R. S. Berry, *Phys. Rev. Lett.* **2004**, *93*, 228104.

[8] D. J. Bonthuis, S. Gekle, R. R. Netz, *Phys. Rev. Lett.* **2011**, *107*, 166102.

[9] G. Lamm, G. R. Pack, *J. Phys. Chem. B* **1997**, *101*, 959

[10] E. Gongadze, A. Iglic, *Bioelectrochemistry* **2012**, *87*, 199

[11] M. Aguilella-Arzo, A. Andrio, V. M. Aguilella, A. Alcaraz, *Phys. Chem. Chem. Phys.* **2009**, *11*, 358.

[12] L. B. Dreier, Y. Nagata, H. Lutz, G. Gonella, J. Hunger, E. H. G. Backus, M. Bonn, *Sci. Adv.* **2018**, *4*, eaap7415.

[13] B. Lee, A. Wan, D. Mastrogiovanni, J. E. Anthony, E. Garfunkel, V. Podzorov, *Phys. Rev. B* **2010**, *82*, 085302.

[14] O. Parlak, S. T. Keene, A. Marais, V. F. Curto, A. Salleo, *Sci. Adv.* **2018**, *4*, eaar2904.

[15] A. Savva, C. Cendra, A. Giugni, B. Torre, J. Surgailis, D. Ohayon, A. Giovannitti, I. McCulloch, E. Di Fabrizio, A. Salleo, J. Rivnay, S. Inal, *Chem. Mater.* **2019**, *31*, 927.

[16] W. Lu, A. G. Fadeev, B. H. Qi, E. Smela, B. R. Mattes, J. Ding, G. M. Spinks, J. Mazurkiewicz, D. Z. Zhou, G. G. Wallace, D. R. MacFarlane, S. A. Forsyth, M. Forsyth, *Science* **2002**, *297*, 983.

[17] H. J. Jang, J. Wagner, H. Li, Q. Zhang, T. Mukhopadhyaya, H. E. Katz, *J. Am. Chem. Soc.* **2019**, *141*, 4861

[18] S. Jamasb, S. D. Collins, R. L. Smith, *IEEE T. Electron Dev.* **1998**, *45*, 1239

[19] L. Bousse, P. Bergveld, *Sens. & Actu.* **1984**, *6*, 65.

[20] J. O. Guardado, A. Salleo, *Adv. Func. Mater.* **2017**, *27*, 1701791

[21] C. Bartic, B. Palan, A. Campitelli, G. Borghs, *Sens. & Actu. B* **2002**, *83*, 115

[22] P. Lin, F. Yan, *Adv. Mater.* **2012**, *24*, 34.

[23] D. A. Bernards, G. G. Malliaras, *Adv. Func. Mater.* **2007**, *17*, 3538.

Figure captions

Figure 1. (a) Schematic image of the RGFET system. Table of measuring media and interface materials on the RG.

Figure 2. V_{th} and G_m distributions with time over 6 samples in pH7 with the RG surface of (a) SiO_2, (b) HMDS, (c) PS, andd (d) PSAA. Schematic image of mechanism in drift regarding (e) orientation ordering on (f) non-polar and (g) acid-functionalized non-polar surface and in (h) hysteresis caused by RSM.

Figure 3. V_{th} and G_m distributions with time over at least 6 samples in ACN with the RG surface of (a) HMDS and (b) PS. Average levels of (c) V_{th0} and V_{sat} (d) ΔV_{dri} and ΔV_{hys} (e) ΔG_{dri} and ΔG_{hys}, respectively, in terms of RG type in ACN.

Figure 4. V_{th} and G_m distributions with time over 6 and 14 samples in pH7 with the RG surface of (a) P3HT and (b) PT-COOH, respectively. V_{th} and G_m distributions over 6 and 8 samples of (c) P3HT and (d) PT-COOH in terms of pH values on time scale, respectively. (e) Comparison in pH response of P3HT and PT-COOH. Average (f) V_{th0}, (g) V_{sat}, (h) ΔV_{dri} and ΔV_{hys} in pH7 in terms of RG type. (i) Average pH sensitivity of each RG over at least 6 samples in terms of RG type.

Table of Contents

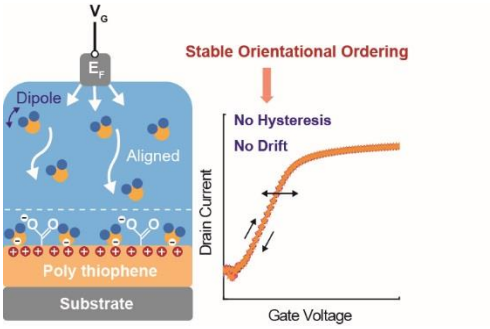

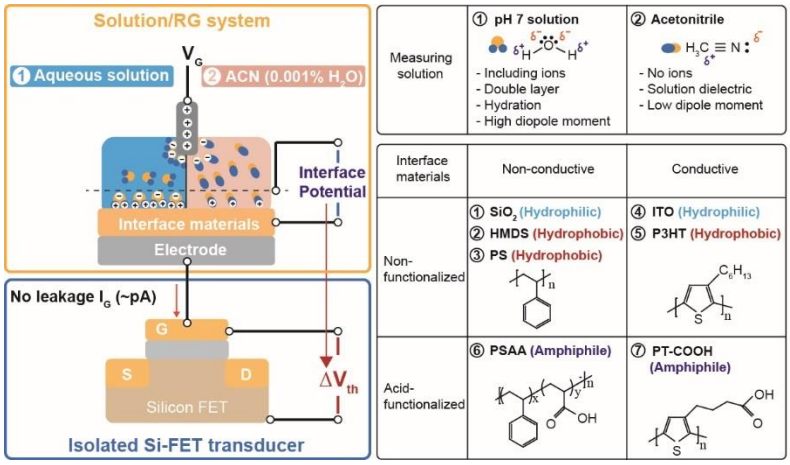
Solution/RG system
V_G
1 Aqueous solution
2 ACN (0.001% H2O)
Interface Potential
Interface materials
Electrode
No leakage I_G (~pA)
G
S
D
ΔV_th
Silicon FET
Isolated Si-FET transducer
Measuring solution
① pH 7 solution
- Including ions
- Double layer
- Hydration
- High diopole moment
② Acetonitrile
- No ions
- Solution dielectric
- Low dipole moment
Interface materials
Non-conductive
Conductive
Non-functionalized
① SiO2 (Hydrophilic)
② HMDS (Hydrophobic)
③ PS (Hydrophobic)
④ ITO (Hydrophilic)
⑤ P3HT (Hydrophobic)
Acid-functionalized
⑥ PSAA (Amphiphile)
⑦ PT-COOH (Amphiphile)

Figure 1

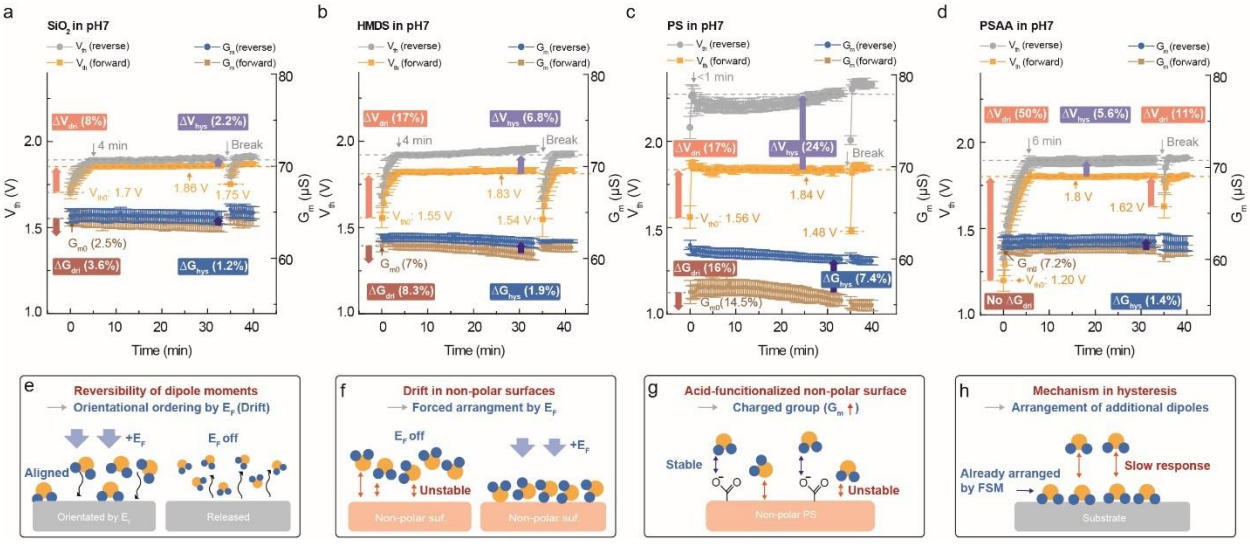
a
SiO2 in pH7
b
HMDS in pH7
c
PS in pH7
d
PSAA in pH7
Time (min)
e
Reversibility of dipole moments
Orientational ordering by EF (Drift)
Aligned
Orientated by EF
Released
f
Drift in non-polar surfaces
Forced arrangment by EF
Unstable
Non-polar suf.
g
Acid-funcitionalized non-polar surface
Charged group (Gm ↑)
Stable
Unstable
Non-polar PS
h
Mechanism in hysteresis
Arrangement of additional dipoles
Already arranged by FSM
Slow response
Substrate

Figure 2

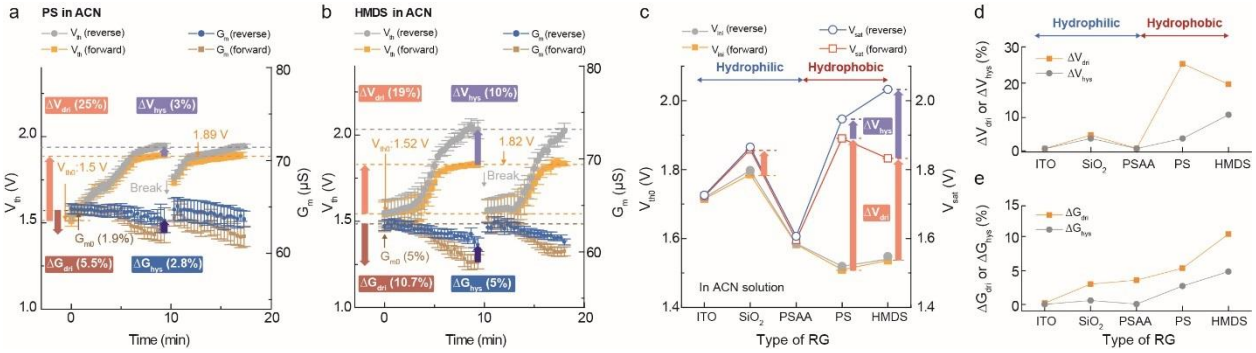
a
PS in ACN
b
HMDS in ACN
c
d
e
Hydrophilic
Hydrophobic
In ACN solution
Time (min)
Type of RG
ITO
PSAA
PS
HMDS

Figure 3

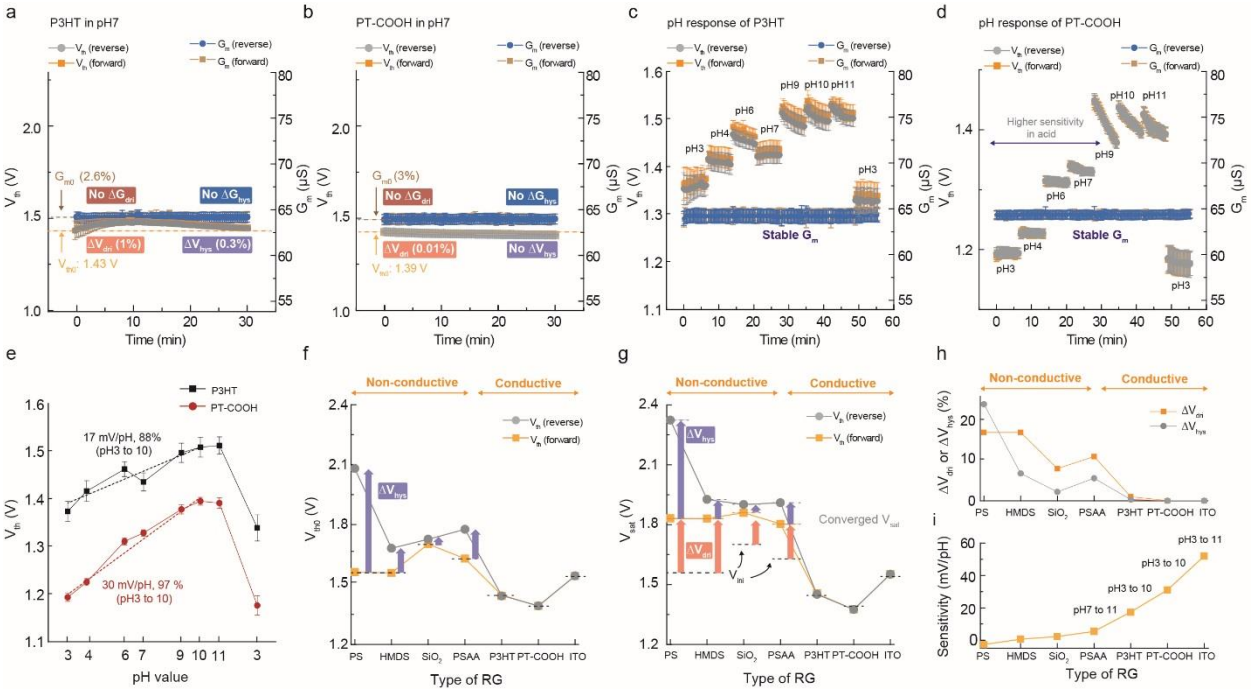
a
P3HT in pH7
b
PT-COOH in pH7
c
pH response of P3HT
d
pH response of PT-COOH
Time (min)
Stable G_m
Higher sensitivity in acid
e
P3HT
PT-COOH
17 mV/pH, 88% (pH3 to 10)
30 mV/pH, 97 % (pH3 to 10)
pH value
f
g
h
Non-conductive
Conductive
Converged V_sat
Type of RG
PS HMDS SiO2 PSAA P3HT PT-COOH ITO
i
Sensitivity (mV/pH)
pH3 to 11
pH3 to 10
pH7 to 11

Figure 4